Available online at www.sciencedirect.com

SCIENCE DIRECT®

Tectonophysics 384 (2004) 115–128

TECTONOPHYSICS

www.elsevier.com/locate/tecto

Fractal distribution of particle size in carbonate cataclastic rocks from the core of a regional strike-slip fault zone

Andrea Billi*, Fabrizio Storti

Dipartimento di Scienze Geologiche, Università "Roma Tre", Largo S.L. Murialdo 1, I-00146 Rome, Italy

Received 14 October 2002; accepted 25 March 2004
Available online 14 May 2004

Abstract

We present particle size data from 31 samples of carbonate cataclastic rocks collected across the 26 m thick fault core of the Mattinata Fault in the foreland of the Southern Apennines, Italy. Particle size distributions of incoherent samples were determined by a sieving-and-weighting technique. The number of weight-equivalent spherical particles by size is well fitted by a power-law function on a log–log space. Fractal dimensions (D) of particle size distributions are in the 2.091–2.932 range and cluster around the value of ~2.5. High D-values pertain to gouge in shear bands reworking the bulk cataclastic rocks of the fault core. Low D-values characterise immature cataclastic breccias. Intermediate D-values are typical of the bulk fault core. Analysis of the ratio between corresponding equivalent particle numbers from differently evolved cataclastic rocks indicates that the development of particle size distributions with D>2.6–2.7 occurred by a preferential relative increase of fine particles rather than a selective decrement of coarse particles. This preferentially occurred in shear bands where intense comminution enhanced by slip localisation progressed by rolling of coarse particles whose consequent smoothing produced a large number of fine particles. Our data suggest that during the progression of cataclasis, the fragmentation mode changed from the Allègre et al.'s [Nature 297 (1982) 47] "pillar of strength" mechanism in the early evolutionary stages, to the Sammis et al.'s [Pure and Applied Geophysics 125 (1987) 777] "constrained comminution" mechanism in the subsequent stages of cataclasis. Eventually, localised shear bands developed mainly by abrasion of coarse particles.

Keywords: Cataclastic rock; Fault core; Fractal dimension; Particle size; Strike-slip fault

1. Introduction

The physical characterisation of cataclastic fault cores is of critical importance for studies of fluid flow (e.g. Takahashi and Abe, 1987; Bear et al., 1993; Hippler, 1993; Antonellini and Aydin, 1994, 1995; Gibson, 1994; Evans et al., 1997; Fisher and Knipe, 1998; Post and Tullis, 1998; Cello et al., 2001; Zhang et al., 2001; Billi et al., 2002; Shipton et al., 2002; Wibberley and Shimamoto, 2003; Ngwenya et al., 2003), and seismic faulting (e.g. Biegel et al., 1989; Beeler et al., 1996; Scott, 1996; Marone, 1998; Scholz, 1998).

The fault core (Fig. 1) is the sector of the fault zone where cataclastic rocks occur and most of the slip is accommodated (Chester et al., 1993; Caine et

* Corresponding author. Tel.: +39-654888016; fax: +39-654888201.
E-mail addresses: billi@uniroma3.it (A. Billi), storti@uniroma3.it (F. Storti).

0040-1951/$ - see front matter © 2004 Elsevier B.V. All rights reserved.
doi:10.1016/j.tecto.2004.03.015

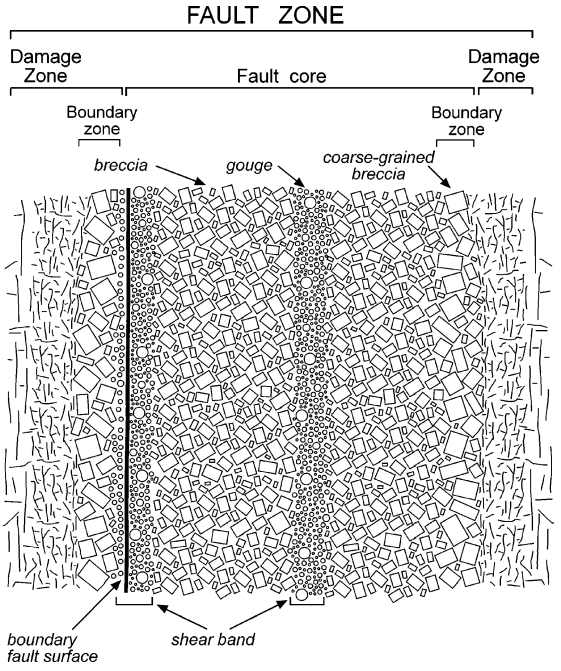

Fig. 1. Conceptual sketch (modified after Storti et al., 2003) of a fault zone sectioned perpendicularly to the boundary fault surface and to the shear direction (i.e. vertical cross-section for a strike-slip fault). The sketch shows the typical asymmetric cross-sectional architecture of a cataclastic fault zone in carbonate rocks (see also Billi et al., 2003b; Storti et al., 2003). The damage zone consists of fractured limestone strata, whereas the fault core consists of cataclastic rocks. A boundary fault borders the fault core on one side (i.e. to the left). Within the fault core, secondary shear bands may develop, locally reworking the cataclastic rocks.

al., 1996). Fault cores are usually surrounded by damage zones consisting of intensely fractured country rocks where pre-existing sedimentary and/or tectonic fabrics are mostly preserved (Caine et al., 1996). The damage zone-fault core transition may abruptly occur by a fault surface or be more gradual through a boundary zone of incipient cataclasis where particle size reduction is dominated by fracturing (Billi et al., 2003a).

Fault core rocks develop by particle comminution with increasing fault displacement. This progressively reduces the size of particles and changes their shape (e.g. Borg et al., 1960; Engelder, 1974; Mandl et al., 1977; Davis, 1999). Analyses of particle size distributions in cataclastic rocks have been widely used to make inferences on the evolution of comminution within fault cores, particularly by correlating natural and experimental data with micromechanical models (Allègre et al., 1982; Turcotte, 1986; Sammis et al., 1987; Marone and Scholz, 1989; Blenkinsop, 1991; Storti et al., 2003). Several studies documented that the particle size distribution of cataclastic rocks can be properly described by fractal laws (e.g. Turcotte, 1986; Sammis et al., 1987; Marone and Scholz, 1989; Sammis and Biegel, 1989) within broad size ranges (e.g. Steacy and Sammis, 1993). The variability of these laws in nature and laboratory experiments suggests that the mechanisms of particle size reduction with fault slip may vary in space and time with varying boundary conditions, and cannot be universally depicted by a single relationship (Blenkinsop, 1991; Storti et al., 2003).

A large amount of particle size data have been collected from natural fault zones (e.g. Engelder, 1974; Aydin, 1978; Aydin and Johnson, 1978; Rutter et al., 1986; Chester and Logan, 1987; Sammis et al., 1987; Blenkinsop, 1991; Chester et al., 1993; Antonellini et al., 1994; Hattori and Yamamoto, 1999; Cashman and Cashman, 2000; Wibberley et al., 2000; Ogilvie and Glover, 2001; White, 2001; Antonellini and Mollema, 2002) and from experimental ones (Shimamoto and Logan, 1981; Sammis et al., 1986; Biegel et al., 1989; Marone and Scholz, 1989; Morrow and Byerlee, 1989; Marone et al., 1990; Marone, 1991; Beeler et al., 1994, 1996; Bos et al., 2000a,b; Mair and Marone, 1999; Mair et al., 2000, 2002; Bos and Spiers, 2001). Most of these data come from low-displacement faults developed in sandstone or in crystalline basement rocks. Much less information is available on carbonate cataclastic rocks (e.g. Olsson, 1974; Vittori et al., 1991; Hadizadeh, 1994; Billi et al., 2003a,b; Storti et al., 2003), particularly from regional scale fault zones.

In this paper, we present particle size data collected in the cataclastic fault core of the Mattinata left-lateral strike-slip fault zone in southern Italy (Fig. 2). The Mattinata Fault cuts across Mesozoic shallow-water carbonate rocks in the foreland of the Apennines thrust-fold belt (Funiciello et al., 1988). We illustrate the distribution of the fractal dimensions (D) from particle size distributions across the Mattinata Fault core, and discuss the relationship between the structural fabric of the fault core and the corresponding particle size distributions of fault rocks. We also discuss the impact of our data on the

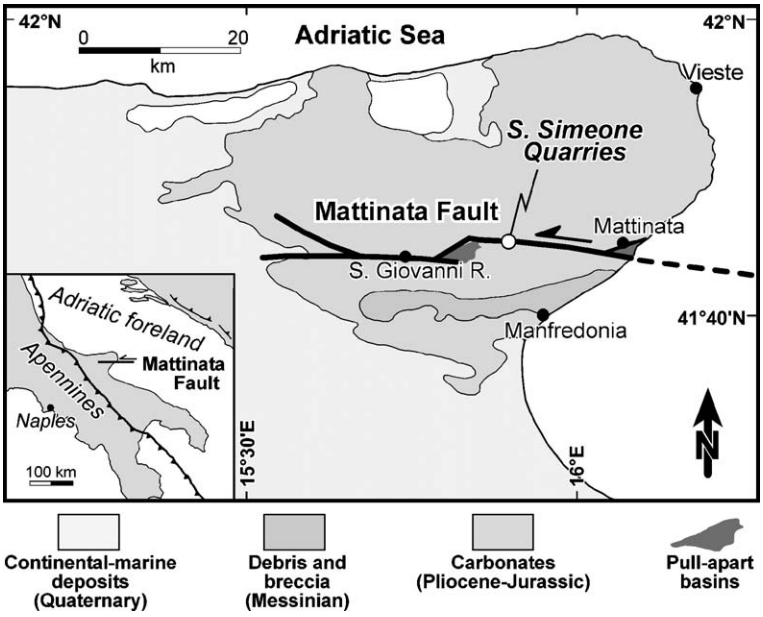

Fig. 2. Location map for the studied fault core situated within the S. Simeone Quarries along the Mattinata Fault, southern Italy.

understanding of the evolution of cataclasis in carbonate rocks.

2. Structural framework

The Mattinata Fault consists of an E–W striking envelope of anastomosed left-lateral strike-slip faults and associated cataclastic rocks (Salvini et al., 1999; Billi and Salvini, 2000, 2001; Brankman and Aydin, 2004). The exposed onshore length of the Mattinata Fault exceeds 45,000 m and its average thickness is about 200 m (Salvini et al., 1999). The displacement can be estimated to be on the order of 2000 m (Billi, 2003). The analysed fault core is exposed along the N–S oriented western wall of the S. Simeone Quarries and has an apparent thickness of ~30 m (Fig. 3a). These quarries locate within a slightly transpressional segment of the Mattinata Fault (Fig. 2). The investigated exposure lies along an active quarry front. The true thickness (i.e. perpendicularly to the boundary fault surface) of the fault core is approximately 26 m. Cataclastic rocks from the analysed fault core are mainly incohesive breccias characterised by rare coarse clasts less than 50 mm in size (Fig. 3b). Secondary left-lateral strike-slip shear bands striking WNW–ESE reworked the cataclastic breccias producing localised reduction of the particle size (Fig. 4). A N121°-striking boundary fault constitutes the southern boundary of the fault core, whereas on the other edge, the fault core changes into the damage zone (Fig. 4a) through a 1–3 m thick transition zone (Fig. 3c). Solution cleavages, extensional fractures and faults occur in the layered-to-massive platform limestone of the damage zone.

3. Particle size analysis

Thirty-one samples (Table 1) of cataclastic rocks were collected from the analysed fault core, starting with the MA1 sample from the gouge within the shear band along the master fault surface, and the MA2 and MA3 samples, respectively, at 0.5 and 1.0 m from MA1. The remainder of the samples (from MA4 to MA31) was collected along the fault core exposure according to a metric succession (Fig. 4b). Although the ongoing quarry activities on the investigated exposure ensured the freshness of the exposed rocks, 10–20 cm of surface cataclastic material were removed from the exposure before sampling. This

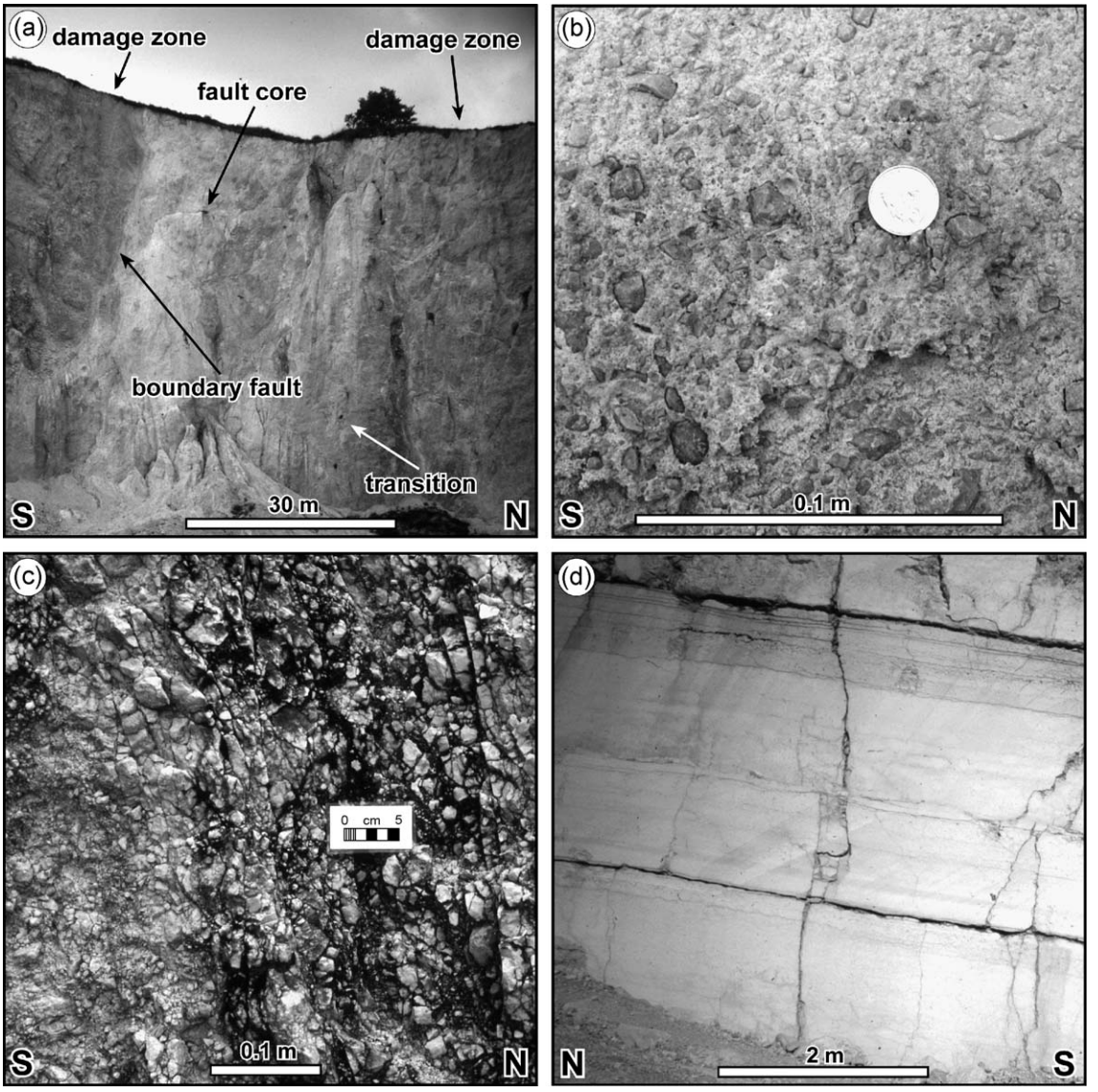

Fig. 3. (a) Photograph of the studied section of the Mattinata Fault core (S. Simeone Quarries). The photograph shows the typical asymmetric structure of the fault zone that consists of (from left to right): the damage zone, the boundary fault, the fault core, the fault core-damage zone transition, and the damage zone. (b) Photograph of poorly indurated cataclastic rocks along the studied fault core. The photograph shows the typical cataclastic fabric that consists of a few coarse clasts entirely surrounded by a fine matrix. (c) Photograph of the fault core-damage zone transition at the northern edge of the studied fault core. Note that pristine vertical cleavage domains are intensely fractured by transverse, sub-horizontal structural surfaces. (d) Photograph of the carbonate protolith as it crops out approximately 500 m to the southwest of the investigated fault core. Note that the protolith shows rare joints and a southwards dip by about 15–20°.

allowed ruling out any possible effect of weathering on the sampled cataclastic rocks.

Particle size distributions were determined by a sieving-and-weighting technique (e.g. Exner, 1972; Anderson et al., 1982; Olgaard and Brace, 1983; Sammis et al., 1986; Hooke and Iverson, 1995) properly modified for this study (Storti et al., 2003). This method consists in disaggregating poorly

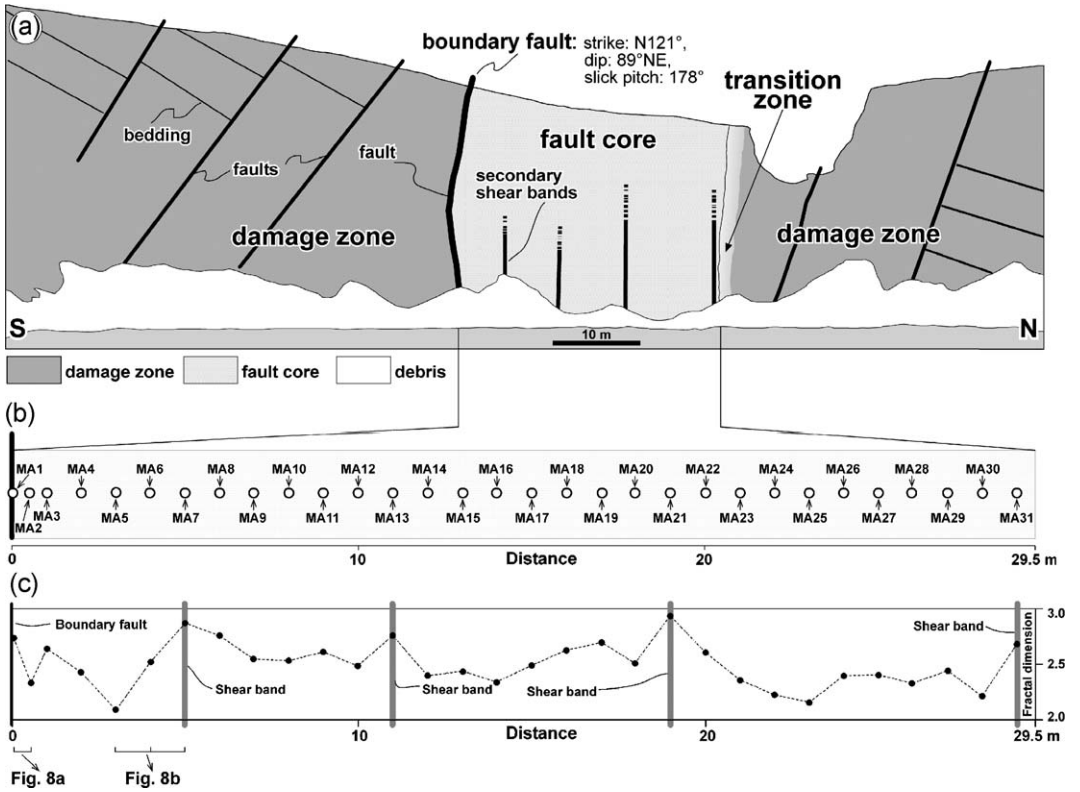

Fig. 4. (a) Line drawing and structural sketch from a photograph of the studied fault core. The structure of the fault zone is similar to the one shown in Fig. 1. Within the fault core, secondary shear bands developed as subvertical gouge zones. (b) Sample location along the fault core. (c) Graph of the fractal dimensions (D) from particle size distributions of fault rock samples against the distance of samples along the fault core exposure. Note that high D-values are associated to the boundary fault and to the secondary shear bands.

cohesive samples in a non-destructive ultrasonic device (Vibra-Cell by Sonics and Materials, Danbury CT, USA) and then drying and sieving them in a standard sieve array consisting of seven sieves with progressively smaller square mesh apertures (i.e. 4.0, 2.0, 1.0, 0.5, 0.25, 0.125 and 0.063 mm). The dry weight of residual material in each sieve was transformed into an equivalent particle number by assuming that the grain shapes can be approximated by spheres (e.g. Hooke and Iverson, 1995). The total weight in each sieve was divided by the weight of the sphere with the same diameter as the mesh aperture of the overlying sieve. A density of 2670 kg/m^3 was used for computing the weight of the reference spheres. The use of different reference values such as the weight of the sphere with the same diameter as the mesh aperture of the underlying sieve, or the weight of the sphere having the average diameter between the mesh apertures of adjacent sieves, does not influence the final distribution of the resulting equivalent particle numbers (Storti et al., 2003). Materials in the largest and smallest sieves were excluded from the procedure because of their intrinsic sampling and sieving limits, respectively. For each sample, the number of equivalent spherical particles of six particle classes was obtained, namely: 4.0, 2.0, 1.0, 0.5, 0.25 and 0.125 mm classes (Table 1). These numbers were plotted against the corresponding particle size classes in log–log graphs (Fig. 5), and the plotted data were fitted by using a power-law function of the type:

$$\log(y) = -D\log(x) + A \quad (1)$$

in which D is the fractal dimension, i.e. the slope of the best-fit line (e.g. Sammis et al., 1986; Turcotte,

Table 1
List of sample data: location, weight, and number of equivalent particles sorted by size class

Sample	Distance [m]	Weight (tot) [g]	Weight (4) [g]	Weight (2) [g]	Weight (1) [g]	Weight (0.5) [g]	Weight (0.25) [g]	Weight (0.125) [g]	Weight (0.063) [g]	Weight (<0.063) [g]	Part.n. (4)	Part.n. (2)	Part.n. (1)	Part.n. (0.5)	Part.n. (0.25)	Part.n. (0.125)
MA1	0	274.21	34.08	38.67	37.91	35.25	27.22	20.94	15.79	64.35	54	424	3152	19,471	119,828	722,857
MA2	0.5	1559.67	1013.06	199.97	121.81	68.74	38.89	26.96	18.92	71.32	279	1361	6146	27,818	154,277	866,146
MA3	1.0	2424.25	923.14	315.16	275.56	217.38	171.42	131.85	89.41	300.33	440	3080	19,437	122,617	754,502	4,093,137
MA4	2.0	920.81	323.09	161.10	127.58	92.67	66.30	11.43	22.40	116.32	225	1426	8286	47,425	65,407	1,025,459
MA5	3.0	1845.63	982.98	351.69	208.65	179.77	66.00	33.53	15.71	7.30	491	2332	16,074	47,210	191,873	719,195
MA6	4.0	2057.36	787.64	425.17	312.74	190.54	104.23	57.34	26.61	113.99	594	3495	17,037	74,556	328,124	1,218,190
MA7	5.0	2100.46	185.53	232.15	271.05	262.97	243.03	203.39	148.67	540.81	324	3029	23,513	173,840	1,163,884	6,806,025
MA8	6.0	2552.22	302.26	331.66	396.64	399.53	325.95	218.73	155.43	422.02	463	4433	35,723	233,153	1,251,666	7,115,493
MA9	7.0	4490.95	898.66	765.06	767.93	651.20	471.77	288.73	167.66	479.94	1069	8583	58,226	337,459	1,652,236	7,675,376
MA10	8.0	2902.34	212.30	479.99	630.15	563.22	377.60	201.31	107.83	302.64	670	7043	50,359	270,099	1,151,982	4,936,394
MA11	9.0	1897.76	279.56	293.57	338.83	303.88	228.31	144.33	78.33	230.95	410	3787	27,171	163,311	825,918	3,585,901
MA12	10.0	1940.89	354.57	350.29	386.27	337.03	222.23	121.91	62.16	106.43	489	4317	30,135	158,962	697,621	2,845,648
MA13	11.0	1231.51	68.16	163.24	226.10	223.13	183.46	118.74	77.72	170.96	228	2527	19,951	131,229	679,481	3,557,976
MA14	12.0	1569.56	319.68	509.31	535.50	410.38	252.15	139.13	67.65	96.73	712	5985	36,693	180,364	796,161	3,096,977
MA15	13.0	833.78	181.34	160.85	166.91	126.45	82.67	47.19	24.42	43.95	225	1865	11,306	59,134	270,041	1,117,933
MA16	14.0	2209.21	731.06	469.22	357.78	239.74	149.64	87.96	48.77	125.04	656	3999	21,436	107,038	503,345	2,232,662
MA17	15.0	1555.37	397.12	286.89	238.80	173.75	123.74	78.82	51.20	205.05	401	2669	15,535	88,512	451,042	2,343,906
MA18	16.0	3245.41	785.50	509.18	484.56	411.12	317.55	217.62	139.77	353.01	711	5416	36,759	227,145	1,245,314	6,398,588
MA19	17.0	1488.08	157.12	216.19	246.20	223.64	181.00	125.59	76.61	234.60	302	2752	19,996	129,470	718,679	3,507,161
MA20	18.0	1409.03	242.53	295.07	278.84	212.15	145.27	90.76	57.40	87.01	412	3116	18,969	103,912	519,367	2,627,738
MA21	19.0	1414.98	88.79	116.47	169.20	186.20	179.55	141.49	94.20	439.08	163	1891	16,649	128,433	809,666	4,312,420
MA22	20.0	1288.94	155.83	211.04	244.83	220.72	164.96	100.27	56.78	134.51	295	2736	19,735	117,996	573,788	2,599,355
MA23	21.0	1671.46	256.07	375.72	378.11	270.69	165.33	87.70	44.24	93.60	525	4226	24,203	118,261	501,857	2,025,281
MA24	22.0	1848.48	449.74	440.63	382.45	256.34	144.03	70.815	32.11	59.61	616	4274	22,920	103,025	405,234	1,469,977
MA25	23.0	2018.26	511.94	539.30	435.74	273.66	144.42	69.03	31.08	52.19	753	4870	24,469	103,304	395,019	1,422,824
MA26	24.0	3264.18	1053.68	618.05	558.95	412.96	258.24	154.38	78.23	102.21	863	6247	36,924	184,720	883,428	3,581,323
MA27	25.0	2460.00	1179.72	389.52	300.98	207.28	137.71	85.57	49.39	82.90	544	3364	18,534	98,504	489,668	2,261,045
MA28	26.0	2232.28	1470.00	275.35	172.58	104.61	69.46	43.79	25.79	43.60	385	1929	9353	49,685	250,585	1,180,651
MA29	27.0	1875.42	792.05	308.03	259.71	191.03	128.77	79.63	45.75	70.45	430	2902	17,081	92,110	455,677	2,094,408
MA30	28.0	3115.39	1791.54	497.26	336.06	203.70	117.51	65.30	33.04	43.57	695	3756	18,213	84,055	373,674	1,512,552
MA31	29.0	999.67	85.53	169.44	221.11	184.23	126.89	73.64	34.67	95.16	947	15,013	156,732	1,044,661	6,164,824	26,095,693

Distance in metres refers to sample location along the fault core, starting from the boundary fault surface (i.e. 0 m). Weight in grams refer to the sample total weight (tot) and to the weight by size classes in millimetres (4), (2), (1), (0.5), (0.25), (0.125), (0.063) and (<0.063). Part.n. is the number of equivalent spherical particles by size classes in millimetres (4), (2), (1), (0.5), (0.25), (0.125), (0.063) and (<0.063).

1986). Statistical parameters describing the power-law best fits are listed in Table 2.

D-values (Fig. 5 and Table 2) vary between a minimum of ~2.09 (MA5) and a maximum of ~2.93 (MA21). By fitting the histogram of *D*-values with an unimodal Gaussian fit (e.g. Salvini et al., 1999), a mean *D*-value of 2.491 (i.e. with a standard deviation (SD) of 0.182) is obtained (Fig. 6). The *D*-population spans around this average value with the exception of a few data, which show values significantly higher or lower than 2.491. In particular, four samples show values greater than 2.73 (i.e. MA1, MA7, MA13, and MA21). These come from 0.10 to 0.25 cm thick gouge layers developed along the boundary fault and characterising the secondary shear bands (Fig. 4c). Samples with *D*-values lower than 2.22 (MA5, MA25 and MA30) come from less evolved cataclastic rocks (sensu Blenkinsop, 1991) that locally occur as coarse-grained breccias.

Sample particles with diameter smaller than 0.063 mm (i.e. those passing through the smallest sieve) are out of the size range considered in the above-discussed fractal analyses. In Fig. 7, their weight divided by the total weight of the sample ($W_{<63}/W_{tot}$) is plotted against the corresponding *D*-value. The data distribu-

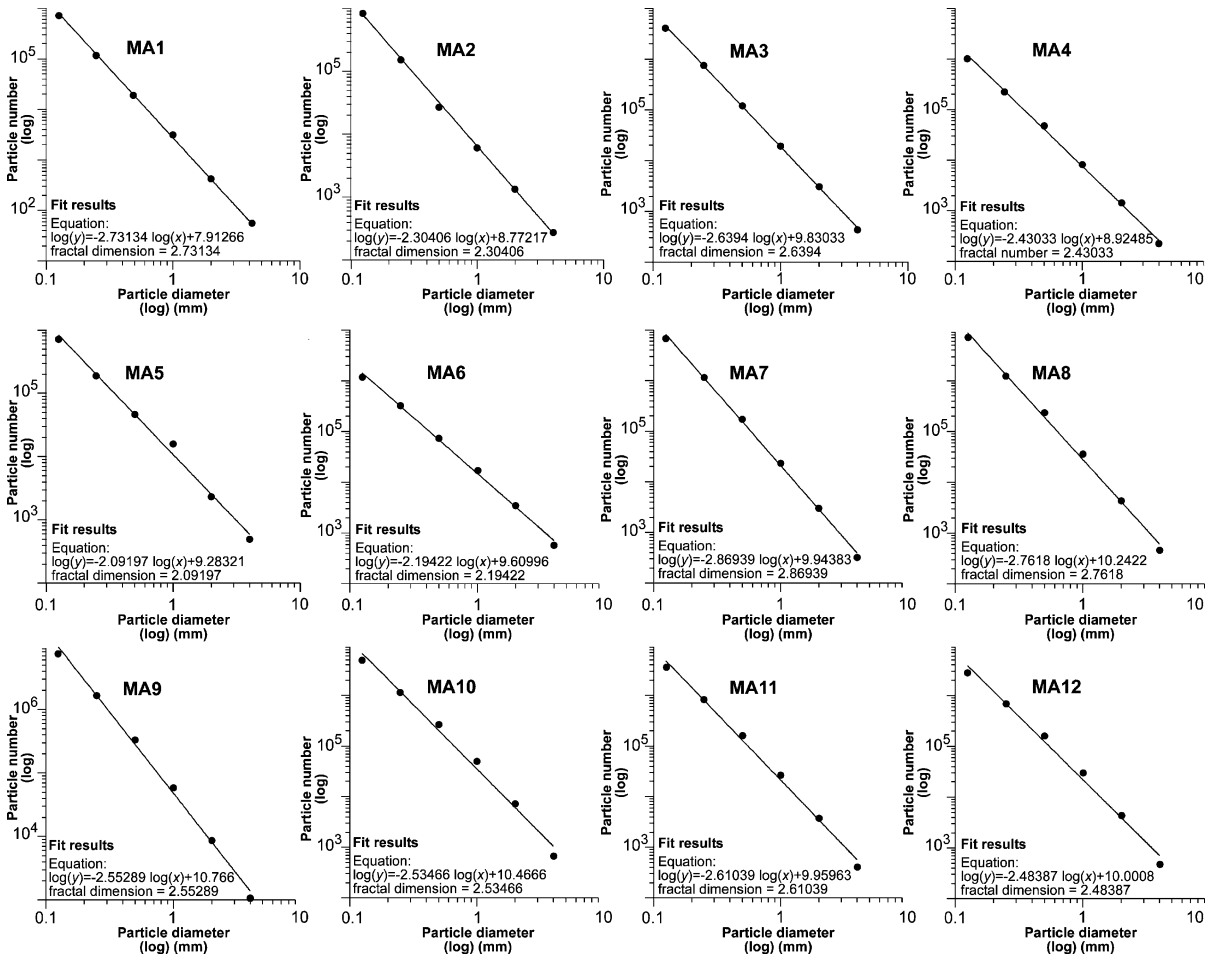

Fig. 5. Log–log graphs showing the numbers of equivalent spherical particles (ordinate) plotted against particle diameters (abscissa) from the sampled cataclastic rocks. In each graph, the power-law best-fit equation and the fractal dimension are provided. Statistical parameters of the best-fit equations are listed in Table 2.

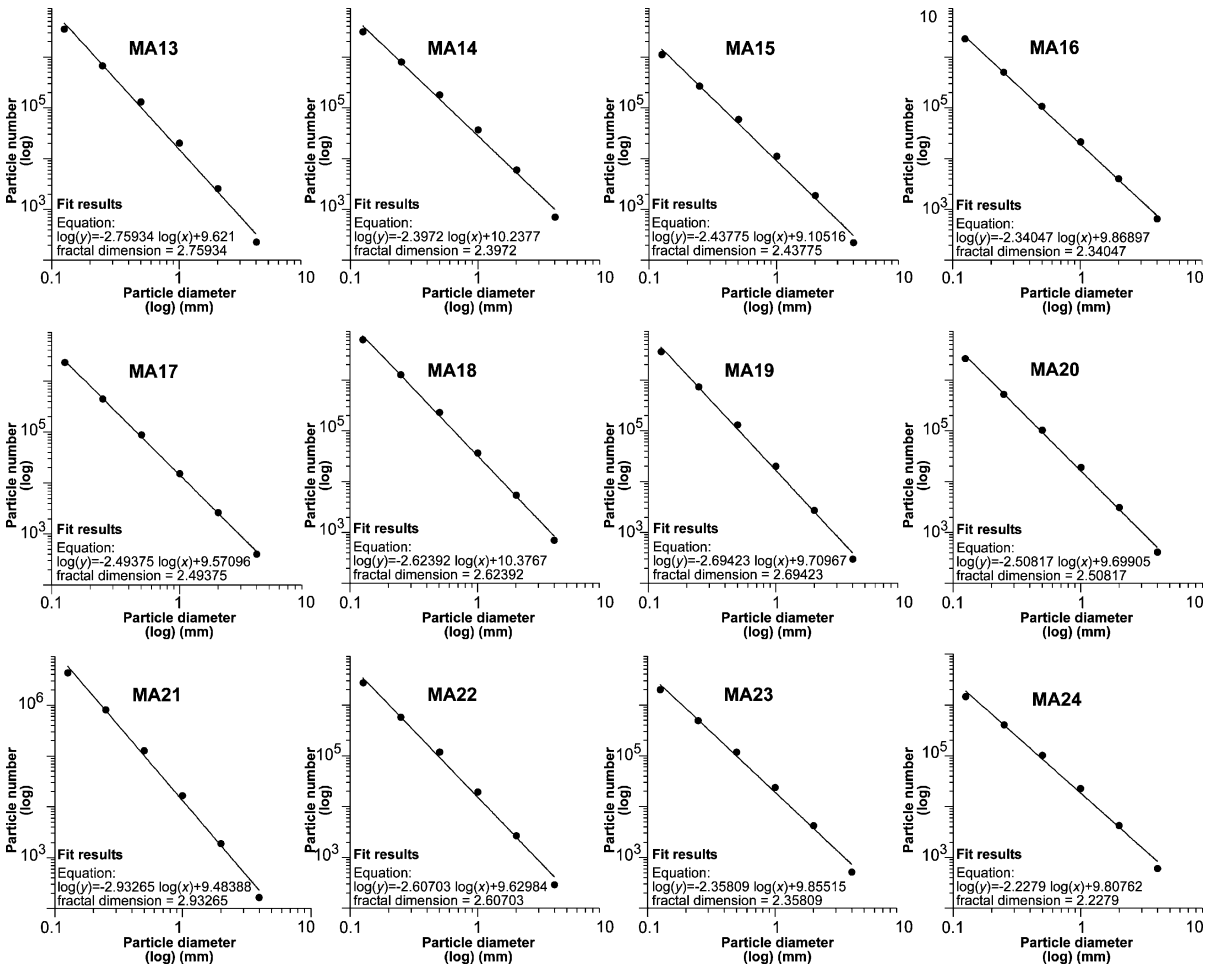

Fig. 5 (*continued*).

tion indicates a general increase of the $W_{<63}/W_{tot}$ ratio (i.e. relative increase of particles less than 0.063 mm in size) with increasing D.

The evolution of the particle size distributions during the overall comminution process can be inferred by comparing the abundance of normalised equivalent particles in corresponding size classes between samples from different locations within the fault core (Storti et al., 2003). We illustrate the variations of normalised equivalent particle numbers in adjacent samples located close to the boundary fault and to one of the shear bands (Fig. 8). Equivalent particle numbers in each size class of the high-D sample were divided by the equivalent particle numbers in the corresponding size class of the low-D sample. This analysis is based on the assumption that the fractal dimension D can be considered an indicator of the comminution degree (Blenkinsop, 1991) and that cataclastic rocks with high D-values developed from cataclastic rocks with low D-values (e.g. Marone and Scholz, 1989; Hattori and Yamamoto, 1999; Storti et al., 2003).

The particle ratio between samples MA1 and MA2 (Fig. 8a) collected close to the boundary fault (Fig. 4), shows that these samples have almost the same abundance of coarse particles (i.e. 4 mm in size). On the contrary, the abundance of fine particles increases more rapidly for the MA1 sample and reaches almost 500% that of the MA2 sample for the 0.063 mm size class. Similar trends are also

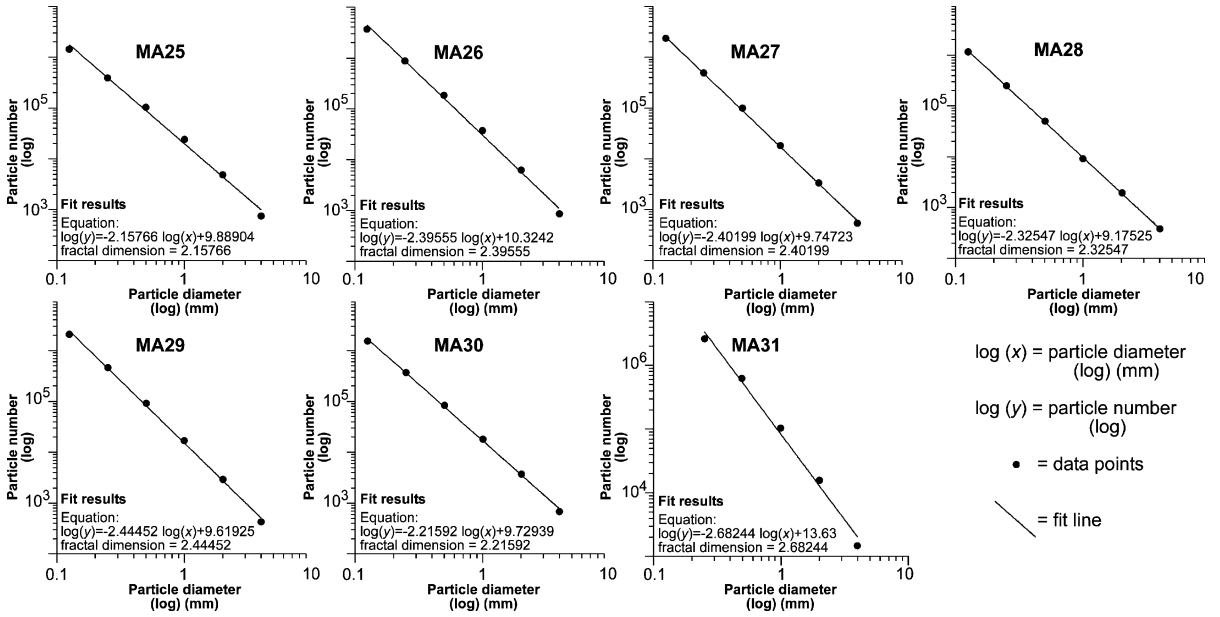

Fig. 5 (*continued*).

observed for the sample pair MA7/MA6 (Fig. 8b), collected within a shear band (MA7) and 1 m away (MA6) (Fig. 4c). In Fig. 8b, we also show the variation of particle abundance between samples MA6 and MA5 collected 1 and 2 m, respectively, from the shear band, and interpreted to be representative of the average fabric of the bulk fault core rocks. This graph (Fig. 8b) shows a greater increase of fine particles for the sample with a high *D*-value (i.e. MA6), but this increment is far less marked than in the adjacent MA7/MA6 sample pair that is closer to the shear band. The abundance of coarse particles in the MA5 and MA6 samples is almost the same.

4. Discussion

Our results show that carbonate cataclastic rocks from the core of the Mattinata Fault have power-law distributions of particle size in the 4.0–0.125 mm interval, with fractal dimensions *D* varying between ~2.09 and ~2.93. Such a large variability of *D*-values contrasts with theoretical values predicted by micromechanical models of fragmentation, according to which *D*-values should be nearly constant during the cataclastic process as dictated by the imposed fragmentation mechanism (Turcotte, 1986). In particular, three main fragmentation mechanisms have been proposed (see Blenkinsop, 1991 for a review): the "pillar of strength" model (Allègre et al., 1982); the "constrained comminution" model (Sammis et al., 1987); and the "plane of fragility" model (Turcotte, 1986). They predicted theoretical *D*-values of 1.97, 2.58 and 2.84, respectively.

An explanation for the observed variability of fractal dimensions may be that fragmentation mechanisms evolved through space and time within the analysed fault core (Storti et al., 2003). In the initial stages of fault core development, when fracturing is the dominant process that leads to particle comminution (e.g. Hallbauer et al., 1973; Sobolev et al., 1978; Billi et al., 2003a), particle size distributions across the fault core may have low fractal dimensions, probably equal to or less than 2.0. This value approximates that predicted by the "pillar of strength" model (Allègre et al., 1982) of rock fragmentation (i.e. *D*=1.97), that is rock failure occurs whenever adjacent fragile domains of rock are arranged such that no pillars of sound material exist. Shear localisation,

Table 2
List of fractal dimensions (D) and of statistical parameters extracted from the power-law best fits of Fig. 5

Sample	Fractal dimension (D)	Regression sum of squares	Residual sum of squares	Coefficient of determination (R^2)	Residual mean square
MA1	2.73134	62.7252	0.0553624	0.999118	0.0138406
MA2	2.30406	44.635	0.0376179	0.999158	0.00940448
MA3	2.63940	58.5733	0.024097	0.999589	0.0060242
MA4	2.43033	41.9993	0.0732181	0.99826	0.024406
MA5	2.09197	36.7959	0.225113	0.993919	0.0562784
MA6	2.19422	40.4807	0.0913108	0.997749	0.0228277
MA7	2.86939	69.2257	0.103674	0.998505	0.0259184
MA8	2.7618	64.1319	0.223808	0.996522	0.0559521
MA9	2.55289	54.7964	0.19654	0.996426	0.0491349
MA10	2.53466	54.0167	0.536468	0.990166	0.134117
MA11	2.61039	57.2927	0.320004	0.994446	0.0800011
MA12	2.48387	51.8735	0.396135	0.992421	0.0990336
MA13	2.75934	64.0176	0.366963	0.9943	0.0917408
MA14	2.3972	48.3168	0.327993	0.993257	0.0819983
MA15	2.43775	49.9654	0.260788	0.994808	0.0651971
MA16	2.34047	46.0571	0.0543055	0.998822	0.0135764
MA17	2.49375	52.2873	0.0394892	0.999245	0.00987229
MA18	2.62392	57.8882	0.0949466	0.998363	0.0237366
MA19	2.69423	61.032	0.211093	0.996553	0.0527732
MA20	2.50817	52.8937	0.10103	0.998094	0.0252576
MA21	2.93265	72.3117	0.328001	0.995485	0.0820002
MA22	2.60703	57.1452	0.321713	0.994402	0.0804282
MA23	2.35809	46.7529	0.270778	0.994242	0.0676944
MA24	2.2279	41.7331	0.245344	0.994155	0.0613361
MA25	2.15766	39.1432	0.199856	0.99492	0.0499641
MA26	2.39555	48.2504	0.169788	0.996493	0.042447
MA27	2.40199	48.5099	0.0420351	0.999134	0.0105088
MA28	2.32547	45.4686	0.00362189	0.99992	0.000905472
MA29	2.44452	50.2432	0.0818343	0.998374	0.0204586
MA30	2.21592	41.2853	0.0388981	0.999059	0.00972452
MA31	2.68244	34.5709	0.270755	0.992229	0.0902518

which would reduce the particle size within the associated shear bands and prevent any further evolution of the bulk fault core (e.g. Storti et al., 2003), is substantially absent at this stage. With progressing the fault displacement, the particle size of the bulk of the fault core rocks reduces and tends towards a size distribution with $D \approx 2.5$. This value is very close to the theoretical 2.58 predicted by the "constrained comminution" model of Sammis et al. (1987), in which the probability of having an adjoining particle of similar size is minimised (see Fig. 3b), and hence also the probability of failure by tensile stresses on coarse particles is reduced. In our dataset, 29 samples out of 31 analysed have particle size distributions with D falling in the $2.58 \pm 15\%$ interval, and 24 have particle size distributions with D falling in the $2.58 \pm 10\%$ interval. Accordingly, fragmentation during the "mature" stage of cataclasis may have substantially progressed according to the "constrained comminution" mechanism of Sammis et al. (1987). Shear localisation along the boundary fault or within the secondary shear bands produced gouge layers characterised by particle size distributions with D=2.7 and probably prevented further evolution of the adjoining cataclastic rocks (Storti et al., 2003). However, the occurrence of cataclastic rocks with D significantly lower than 2.58 (Fig. 4c) suggests that, in places, shear localisation occurred before the entire fault core reached a "mature" particle size distribution of rocks, i.e. with $D \approx 2.58$.

Rotation-enhanced particle abrasion is another important mechanism that may have contributed to

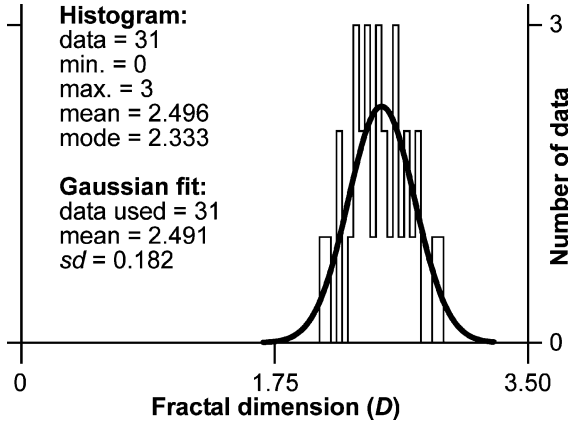

Fig. 6. Histogram and Gaussian best fit of *D*-values (31 data) obtained from particle size analyses of the studied cataclastic rocks.

determine the size distribution of cataclastic rock particles (e.g. Hooke and Iverson, 1995; Morgan et al., 1997). Particle abrasion produces the preferential increase of the relative content of fine particles with respect to the content of coarse particles, and hence it causes an increase of *D*-values (Storti et al., 2003). This is corroborated by our results showing that in differently evolved cataclastic rocks (i.e. different *D*-values), particle size distributions undergo a preferential relative increase of fine particles rather than a selective decrement of coarse particles (Fig. 8). The increase of the content in particles less than 0.063 mm in size with increasing *D*-values (Fig. 7) provides further support to the increased importance of particle abrasion with progressing cataclasis in fault core rocks of the Mattinata Fault. Accordingly, particle abrasion is likely negligible in the early evolutionary stages of fault core rocks and its role becomes more important with increasing fault slip, being eventually fundamental in intensely comminuted shear bands, where interpretation of *D*-values solely in terms of fragmentation models is probably misleading.

5. Conclusions

We analysed particle size distributions of carbonate cataclastic rocks collected in the fault core of the regionally sized, left-lateral strike-slip Mattinata Fault in southern Italy. Our results show that particle size distributions of fault rocks are well fitted by power-law best fits over the 4.0–0.125 mm size interval. Fractal dimensions (*D*) vary between ~2.09 and ~2.93. In particular, *D*-values increase from a mean value of ~2.5 in the bulk fault core, to values higher than 2.7 in the gouge associated to the boundary fault and to the shear bands reworking the "mature" cataclastic fabric. The development of particle size distributions with $D>2.6–2.7$ occurred by the preferential relative increase of fine particles rather than by the selective decrement of coarse particles. Minimum *D*-values (i.e. close to 2) occur in poorly evolved breccias situated away from the boundary fault surface and from the shear bands. Such a spatial distribution of fault rocks with different particle size distributions suggests that the cataclastic process involved different comminution mechanisms through time and space: (i) fragmentation according to the "pillar of strength" mechanism (Allègre et al., 1982) occurred in the early stages of cataclasis; (ii) with progressing fault displacement and cataclasis, the fragmentation mechanism changed into the "constrained comminution" of Sammis et al. (1987); (iii) eventually, shear localisation enhanced rolling-induced

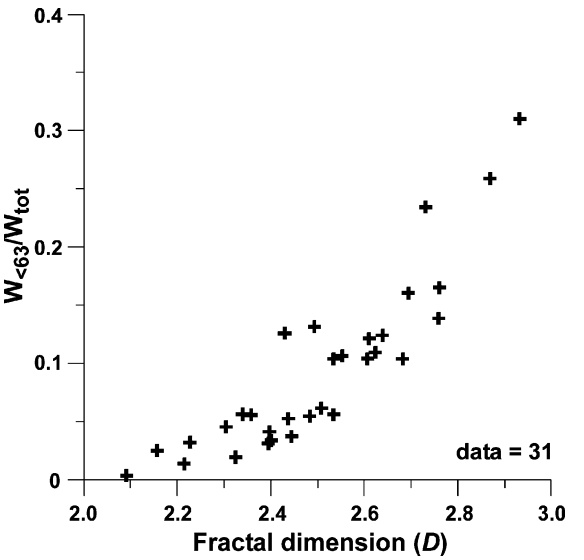

Fig. 7. Graph showing the weight of particles smaller than 0.063 mm in size divided by the total weight of the sample ($W_{<63}/W_{tot}$), plotted against the corresponding value of *D*.

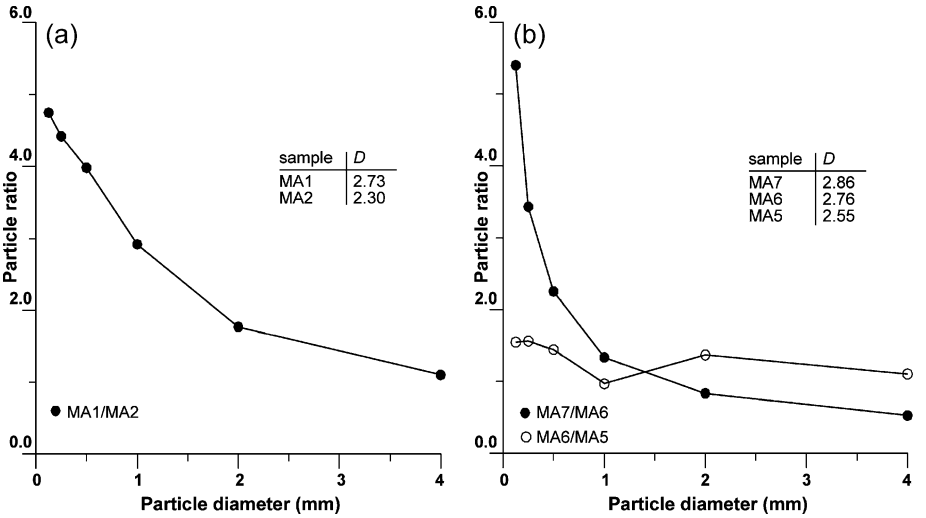

Fig. 8. Ratios between the equivalent particle numbers in corresponding size classes of adjacent samples collected (a) close to the boundary fault and (b) close to a shear band. See Fig. 4c for location of samples analysed in these graphs. Note that the numbers of particles are normalised to 1000 g of sampled material.

particle abrasion and the formation of extremely fine-grained gouge layers.

Acknowledgements

Encouragements for this study derive from an early research project funded by Enterprise Oil and coordinated by F. Salvini, to whom we are in debt for useful suggestions and advice. Reviews by T. Blenkinsop and J. Hadizadeh significantly improved the science of the paper.

References

Allègre, C.J., Le Mouel, J.L., Provost, A., 1982. Scaling rules in rock fracture and possible implications for earthquake prediction. Nature 297, 47–49.

Anderson, J.L., Osborne, R.H., Palmer, D.F., 1982. Petrogenesis of cataclastic rock within the San Andreas fault zone of southern California. Tectonophysics 67, 221–249.

Antonellini, M., Aydin, A., 1994. Effect of faulting on fluid flow in porous sandstones: petrophysical properties. American Association of Petroleum Geologists Bulletin 78, 355–377.

Antonellini, M., Aydin, A., 1995. Effect of faulting on fluid flow in porous sandstones: geometry and spatial distribution. American Association of Petroleum Geologists Bulletin 79, 642–671.

Antonellini, M., Mollema, P., 2002. Cataclastic faults in the Loiano Sandstones; Northern Apennines, Italy. Bollettino della Società Geologica Italiana 121, 163–178.

Antonellini, M., Aydin, A., Pollard, D.D., 1994. Microstructure of deformation bands in porous sandstones at Arches National Park, Utah. Journal of Structural Geology 16, 941–959.

Aydin, A., 1978. Small faults formed as deformation bands in sandstone. Pure and Applied Geophysics 116, 913–930.

Aydin, A., Johnson, A.M., 1978. Development of faults as zones of deformation bands and as slip surfaces in sandstone. Pure and Applied Geophysics 116, 931–942.

Bear, J., Tsang, C., de Marsily, G., 1993. Flow and Contaminant Transport in Fractured Rock. Academic Press, San Diego.

Beeler, N.M., Tullis, T.E., Weeks, J.D., 1994. The roles of time and displacement in the evolution effect in rock friction. Geophysical Research Letters 21, 1987–1990.

Beeler, N.M., Tullis, T.E., Blanpied, M.L., Weeks, J.D., 1996. Frictional behavior of large displacement experimental faults. Journal of Geophysical Research 101, 8697–8715.

Biegel, R.L., Sammis, C.G., Dieterich, J.H., 1989. The frictional properties of a simulated gouge having a fractal particle distribution. Journal of Structural Geology 11, 827–846.

Billi, A., 2003. Solution slip and separations on strike-slip fault zones: theory and application to the Mattinata Fault, Italy. Journal of Structural Geology 25, 703–715.

Billi, A., Salvini, F., 2000. Sistemi di fratture associati a faglie in rocce carbonatiche: nuovi dati sull'evoluzione tettonica del Promontorio del Gargano. Bollettino della Società Geologica Italiana 119, 237–250.

Billi, A., Salvini, F., 2001. Fault-related solution cleavage in exposed carbonate reservoir rocks in the southern Apennines, Italy. Journal of Petroleum Geology 24, 147–169.

Billi, A., Salvini, F., Storti, F., 2002. Petrophysical characterisation

of fault zones in carbonate rocks: implications for the evolution of structural and permeability properties. Bollettino di Geofisica Teorica ed Applicata 42, 271–274.

Billi, A., Salvini, F., Storti, F., 2003. The damage zone-fault core transition in carbonate rocks: implications for fault growth, structure and permeability. Journal of Structural Geology 25, 1779–1794.

Billi, A., Storti, F., Salvini, F., 2003. Particle size distribution of fault rocks and fault transpression: are they related? Terra Nova 15, 61–66.

Blenkinsop, T.G., 1991. Cataclasis and processes of particle size reduction. Pure and Applied Geophysics 136, 59–86.

Borg, I., Friedman, M., Handin, J., Higgs, D.V., 1960. Experimental deformation of St. Peter sand: a study of cataclastic flow. Memoir-Geological Society of America 79, 133–191.

Bos, B., Spiers, C.J., 2001. Experimental investigation into the microstructural and mechanical evolution of phyllosilicate-bearing fault rock under conditions favouring pressure solution. Journal of Structural Geology 23, 1187–1202.

Bos, B., Peach, C.J., Spiers, C.J., 2000. Frictional-viscous flow of simulated fault gouge caused by the combined effects of phyllosilicates and pressure solution. Tectonophysics 327, 173–194.

Bos, B., Peach, C.J., Spiers, C.J., 2000. Slip behavior of simulated gouge-bearing faults under conditions favoring pressure solution. Journal of Geophysical Research 105, 16699–16717.

Brankman, C.M., Aydin, A., 2004. Uplift and contractional deformation along a segmented strike-slip fault system: the Gargano Promontory, southern Italy. Journal of Structural Geology 26, 807–824.

Caine, J.S., Evans, J.P., Forster, C.B., 1996. Fault zone architecture and permeability structure. Geology 24, 1025–1028.

Cashman, S., Cashman, K., 2000. Cataclasis and deformation-band formation in unconsolidated marine terrace sand, Humboldt County, California. Geology 28, 111–114.

Cello, G., Tondi, E., Micarelli, L., Invernizzi, C., 2001. Fault zone fabrics and geofluid properties as indicators of rock deformation modes. Journal of Geodynamics 32, 543–565.

Chester, F.M., Logan, J.M., 1987. Composite planar fabric of gouge from the Punchbowl Fault, California. Journal of Structural Geology 9, 621–634.

Chester, F.M., Evans, J.P., Biegel, R.L., 1993. Internal structure and weakening mechanisms of the San Andreas Fault. Journal of Geophysical Research 98, 771–786.

Davis, G.H., 1999. Structural geology of the Colorado Plateau region of southern Utah, with special emphasis on deformation bands. Special Paper, Geological Society of America 342, 1–156.

Engelder, J.T., 1974. Cataclasis and the generation of fault gouge. Geological Society of America Bulletin 85, 1515–1522.

Evans, J.P., Forster, C.B., Goddard, J.V., 1997. Permeabilities of fault-related rocks and implications for fault-zone hydraulic structure. Journal of Structural Geology 19, 1393–1404.

Exner, H.E., 1972. Analysis of grain- and particle-size distributions in metallic materials. International Metallurgical Reviews 17, 25–42.

Fisher, Q.J., Knipe, R.J., 1998. Fault sealing processes in siliciclastic sediments. In: Jones, G., Fisher, Q.J., Knipe, R.J. (Eds.), Faulting, Fault Sealing and Fluid Flow in Hydrocarbon Reservoirs. Special Publication-Geological Society, vol. 147, pp. 117–135.

Funiciello, R., Montone, P., Salvini, F., Tozzi, M., 1988. Caratteri strutturali del Promontorio del Gargano. Memorie della Società Geologica Italiana 41, 1235–1243.

Gibson, R.G., 1994. Fault-zone seals in siliciclastic strata of the Columbus basin, Offshore Trinidad. American Association of Petroleum Geologists Bulletin 78, 1372–1385.

Hadizadeh, J., 1994. Interaction of cataclasis and pressure solution in a low-temperature carbonate shear zone. Pure and Applied Geophysics 143, 255–280.

Hallbauer, D.K., Wagner, H., Cook, N.G.W., 1973. Some observations concerning the microscopic and mechanical behaviour of quartzite specimens in stiff, triaxial compression tests. International Journal of Rock Mechanics and Mining Sciences & Geomechanics Abstracts 10, 713–726.

Hattori, I., Yamamoto, H., 1999. Rock fragmentation and particle size in crushed zones by faulting. Journal of Geology 107, 209–222.

Hippler, S.J., 1993. Deformation microstructures and diagenesis in sandstone adjacent to an extensional fault: implications for the flow and entrapment of hydrocarbons. American Association of Petroleum Geologists Bulletin 77, 625–637.

Hooke, R.LeB., Iverson, N.R., 1995. Grain-size distribution in deforming subglacial tills: role of grain fracture. Geology 23, 57–60.

Mair, K., Marone, C., 1999. Friction of simulated fault gouge for a wide range of velocities and normal stresses. Journal of Geophysical Research 104, 28899–28914.

Mair, K., Main, I., Elphick, S., 2000. Sequential growth of deformation bands in the laboratory. Journal of Structural Geology 22, 25–42.

Mair, K., Elphick, S., Main, I., 2002. Influence on confining pressure on the mechanical and structural evolution of laboratory deformation bands. Geophysical Research Letters 29, 1410 (doi: 10.1029/2001GL013964).

Mandl, G., de Jong, L.N.J., Maltha, A., 1977. Shear zones in granular material—an experimental study of their structure and mechanical genesis. Rock Mechanics 9, 95–144.

Marone, C., 1991. A note on the stress-dilatancy relation for simulated fault gouge. Pure and Applied Geophysics 137, 409–419.

Marone, C., 1998. Laboratory-derived friction laws and their application to seismic faulting. Annual Review of Earth and Planetary Science Letters 26, 643–696.

Marone, C., Scholz, C.H., 1989. Particle-size distribution and microstructures within simulated fault gouge. Journal of Structural Geology 11, 799–814.

Marone, C., Raleigh, C.B., Scholz, C.H., 1990. Frictional behavior and constitutive modeling of simulated fault gouge. Journal of Geophysical Research 95, 7007–7025.

Morgan, K.J., Cladouhos, T.T., Scharer, K.M., Cowan, D.S., Vrolijk, P., 1997. Fractal particle size distributions in Death Valley fault zones: controls on mechanics and kinematics of fault rocks. Abstracts of Proceedings, AGU Fall Meeting.

Morrow, C.A., Byerlee, J.D., 1989. Experimental studies of compaction and dilatancy during frictional sliding on faults containing gouge. Journal of Structural Geology 11, 815–825.

Ngwenya, B.T., Kwon, O., Elphick, S.C., Main, I.G., 2003. Permeability evolution during progressive development of deformation bands in porous sandstones. Journal of Geophysical Research 108, 2343 (doi: 10.1029/2002JB001854).

Ogilvie, S.R., Glover, P.W.J., 2001. The petrophysical properties of deformation bands in relation to their microstructure. Earth and Planetary Science Letters 193, 129–142.

Olgaard, D.L., Brace, W.F., 1983. The microstructure of gouge from a mining-induced seismic shear zone. International Journal of Rock Mechanics and Mining Sciences & Geomechanics Abstracts 20, 11–19.

Olsson, W.A., 1974. Microfracturing and faulting in a limestone. Tectonophysics 24, 277–285.

Post, A., Tullis, J., 1998. The rate of water penetration in experimentally deformed quartzite: implications for hydrolytic weakening. Tectonophysics 295, 117–137.

Rutter, E.H., Maddock, R.H., Hall, S.H., White, S.H., 1986. Comparative microstructures of natural and experimentally produced clay-bearing fault gouges. Pure and Applied Geophysics 124, 3–29.

Salvini, F., Billi, A., Wise, D.U., 1999. Strike-slip fault-propagation cleavage in carbonate rocks: the Mattinata Fault zone. Journal of Structural Geology 21, 1731–1749.

Sammis, C.G., Biegel, R., 1989. Fractals, fault gouge, and friction. Pure and Applied Geophysics 131, 256–271.

Sammis, C.G., Osborne, R.H., Anderson, J.L., Banerdt, M., White, P., 1986. Self-similar cataclasis in the formation of fault gouge. Pure and Applied Geophysics 124, 53–78.

Sammis, C.G., King, G., Biegel, R., 1987. The kinematics of gouge deformation. Pure and Applied Geophysics 125, 777–812.

Scholz, C.H., 1998. Earthquakes and friction laws. Nature 391, 37–42.

Scott, D.R., 1996. Seismicity and stress rotation in a granular model of the brittle crust. Nature 381, 592–595.

Shimamoto, T., Logan, J.M., 1981. Effects of simulated fault gouge on the sliding behavior of Tennessee sandstone: nonclay gouges. Journal of Geophysical Research 86, 2902–2914.

Shipton, Z.K., Evans, J.P., Robeson, K.R., Forster, C.B., Snelgrove, S., 2002. Structural heterogeneity and permeability in faulted eolian sandstone: implications for subsurface modeling of faults. American Association of Petroleum Geologists 86, 863–883.

Sobolev, G., Spetzler, H., Salov, B., 1978. Precursors to failure in rocks while undergoing anelastic deformation. Journal of Geophysical Research 83, 1775–1784.

Steacy, S.A., Sammis, C.G., 1993. A damage mechanics model for fault zone friction. Journal of Geophysical Research 97, 587–594.

Storti, F., Billi, A., Salvini, F., 2003. Particle size distributions in natural carbonate fault rocks: insights for non-self-similar cataclasis. Earth and Planetary Science Letters 206, 173–186.

Takahashi, H., Abe, A., 1987. Fracture mechanics applied to hot, dry rock geothermal energy. In: Atkinson, B.K. (Ed.), Fracture Mechanics of Rock. Academic Press, London, pp. 241–276.

Turcotte, D.L., 1986. Fractals and fragmentation. Journal of Geophysical Research 91, 1921–1926.

Vittori, E., Cavinato, G.P., Miccadei, E., Rughi, D., Serva, L., 1991. First results of a study on cataclastic and intense fracturing processes in calcareous rocks (Central Apennines, Italy). Bollettino della Società Geologica Italiana 110, 489–499.

White, S.R., 2001. Textural and microstructural evidence for semibrittle flow in natural fault rocks with varied mica contents. International Journal of Earth Sciences 90, 14–27.

Wibberley, C.A.J., Shimamoto, T., 2003. Internal structure and permeability of major strike-slip fault zones: the Median Tectonic Line in Mie Prefecture, Southwest Japan. Journal of Structural Geology 25, 59–78.

Wibberley, C.A.J., Petit, J.-P., Rives, T., 2000. Mechanics of cataclastic "deformation band" faulting in high-porosity sandstone, Provence. Comptes Rendus de l'Academie des Sciences Series IIA Earth and Planetary Science 331, 419–425.

Zhang, S., Tullis, T.E., Scruggs, V.J., 2001. Implications of permeability and its anisotropy in a mica gouge for pore pressures in fault zones. Tectonophysics 335, 37–50.